John von Neumann Institute for Computing

Quantum Monte Carlo Studies of Correlated Systems

C. Lavalle, M. Arikawa, S. Capponi, A. Muramatsu

published in

NIC Symposium 2004, Proceedings,
Dietrich Wolf, Gernot Münster, Manfred Kremer (Editors),
John von Neumann Institute for Computing, Jülich,
NIC Series, Vol. **20**, ISBN 3-00-012372-5, pp. 281-290, 2003.

http://www.fz-juelich.de/nic-series/volume20

Quantum Monte Carlo Studies of Correlated Systems

C. Lavalle[1], M. Arikawa[1], S. Capponi[2], and A. Muramatsu[1]

[1] Institut für Theoretische Physik III
Universität Stuttgart, 70550 Stuttgart, Germany
E-mail: {lavalle,arikawa,mu}@theo3.physik.uni-stuttgart.de

[2] Laboratoire de Physique Quantique
Université Paul Sabatier, 118 route de Narbonne, 31062 Toulouse, France
E-mail: capponi@irsamc.ups-tlse.fr

A new quantum Monte Carlo (QMC) algorithm to simulate electronic systems in the limit of strong correlations will be presented. Specifically, we deal with the t-J model, that is currently at the center of attention of theoretical studies of high temperature superconductors and related strongly correlated compounds, where the interplay of charge and spin degrees of freedom is essential for their understanding. The spin degrees of freedom are treated with a loop-algorithm that allows for global updates of spin configurations whereas for each spin configuration, the evolution of the charge degrees of freedom is calculated exactly by means of a determinantal algorithm. Hence, we denominate the whole as a hybrid-loop algorithm.

1 Introduction

Triggered by the discovery of high temperature superconductors[1] (HTS), a pletora of new systems were discovered[2], where the correlated dynamics of the spin and charge degrees of freedom of the electrons resist up to now a theoretical understanding.

The essential physical properties of correlated materials are in essence represented by the Hubbard or the t-J model[3]. The Hubbard model describes electrons on a lattice that can tunnel from site to site with an amplitude t, and with an on-site interaction U. Although rather simple, this model shows a metal-insulator transition at commensurate fillings and magnetic phases, as observed in many correlated materials. In the limit of strong correlations ($U \gg t$), electrons will avoid occupied sites and a new energy scale $J \sim t^2/U$ appears, that corresponds to an antiferromagnetic exchange interaction between electrons on neighboring sites. This is the regime described by the t-J model, that constitutes the minimal model for HTS. Away from density $n = 1$ (i.e. on average one electron per site), not much is known about these models. Even in one dimension, where ground-state and thermodynamic properties of the Hubbard model can be obtained exactly[4], correlation and spectral functions are very difficult to compute. The situation is worse in two dimensions, where no controlled theoretical methods are yet available. However, progress was made recently in infinite dimensions or within the so-called dynamical mean-field theory (DMFT)[5]. Due to the avoidance of doubly occupied sites, the t-J model has a reduced Hilbert space with respect to the Hubbard model, such that larger system sizes can be exactly diagonalized[6]. However, since the dimension of the Hilbert space increases exponentially with the system size, such studies are limited to very small systems (approx. 30 sites), whereas the anomalies observed experimentally correspond to the thermodynamic limit. It is therefore very important to develop accurate methods able to deal with rather large systems, such that finite size extrapolations become possible, in order to access the physics on the macroscopic scale.

2 The t-J Model and the Hybrid-Loop Algorithm

The nearest neighbor (NN) t-J model is given by the following Hamiltonian in second quantization:

$$H_{t-J} = -t \sum_{<i,j>\sigma} (\tilde{c}^{\dagger}_{i,\sigma}\tilde{c}_{j,\sigma} + \text{h.c.}) + J \sum_{<i,j>} \left(\vec{S}_i \cdot \vec{S}_j - \frac{1}{4}\tilde{n}_i\tilde{n}_j \right), \tag{1}$$

where $\tilde{c}^{\dagger}_{i,\sigma}$ are projected fermion creation operators $\tilde{c}^{\dagger}_{i,\sigma} = (1 - n_{i,-\sigma})c^{\dagger}_{i,\sigma}$, while $c^{\dagger}_{i,\sigma}$ and $c_{i,\sigma}$ are canonical creation and annihilation fermionic operators respectively, and $n_{i,\sigma} = c^{\dagger}_{i,\sigma}c_{i,\sigma}$ gives the density of electrons with spin σ. In the same way, a projected density operator $\tilde{n}_i = \sum_{\alpha} \tilde{c}^{\dagger}_{i,\alpha}\tilde{c}_{i,\alpha}$ can be defined. $\vec{S}_i = (1/2)\sum_{\alpha,\beta} c^{\dagger}_{i,\alpha}\vec{\sigma}_{\alpha,\beta}c_{i,\beta}$ describes the spin degrees of freedom. Finally, $< i,j >$ denotes the bond between nearest neighbor sites i and j. The projector $(1 - n_{i,-\sigma})$ allows to create an electron with spin σ at site i only if there is no other electron on that site. Such a constraint reflects the strongly correlated nature of the particles and leads to a reduction of the Hilbert space by one state per site.

A number of so-called world-line algorithms were developed for the t-J model[7–9]. There, the partition function of the system in d dimensions is mapped onto a $d+1$ dimensional system, where the extra dimension is denoted "imaginary time"[10,11]. The evolution of the system in this "space-time" is described by world-lines that resemble polymers streched in the extra dimension (Fig. 1). The earlier versions resticted to local moves[7] were superseeded by new loop-algorithms[8,9], with global moves and not restricted to a given charge or spin sector. World-line algorithms for fermions suffer under the *minus sign* problem, where large contributions with different signs lead to large fluctuations as the system size increases or the temperature is lowered. This problem is less severe in one dimension, and can be avoided in special cases like for one hole and $J = 0$ in two dimensions[9] or for single-hole excitations on a non-frustrated quantum antiferromagnet in any dimension[12–14]. A recent advance on the *minus sign* problem was achieved by the Green's function Monte Carlo with stochastic reconfiguration (GFMCSR)[15]. However, this algorithm is not exact, and an accurate determination of correlation functions is difficult.

An advantageous separation of electrons in spin and charge variables is achieved by a canonical transformation[16,17]

$$c^{\dagger}_{i\uparrow} = \gamma^{+}_i f_i - \gamma^{-}_i f^{\dagger}_i\,, \quad c^{\dagger}_{i\downarrow} = \sigma^{-}_i (f_i + f^{\dagger}_i)\,, \tag{2}$$

where $f^{\dagger}_i, f_i$ are canonical operators for spinless fermions, $\sigma^{\pm} = 1/2(\sigma^x \pm i\sigma^y)$, and $\gamma^{\pm} = 1/2(1 \pm \sigma^z)$, with $\sigma^{\alpha},\ \alpha = x,y,z$ Pauli matrices. The Hamiltonian in the new representation becomes

$$\mathcal{H} = +t \sum_{<i,j>} P_{ij} f^{\dagger}_i f_j + \frac{J}{2} \sum_{<i,j>} \Delta_{ij}(P_{ij} - 1), \tag{3}$$

where $P_{ij} = 1/2(1 + \vec{\sigma}_i \cdot \vec{\sigma}_j)$ and $\Delta_{ij} = 1 - f^{\dagger}_i f_i - f^{\dagger}_j f_j$. The constraint against double occupancy becomes $\sum_i (1 - \sigma^z_i) f^{\dagger}_i f_i = 0$, and commutes with the Hamiltonian. We consider now the following definition of an expectation value:

$$\langle \hat{\mathcal{O}} \rangle = \lim_{\Theta \to \infty} \frac{\sum_n \langle \Psi_n \mid \mathcal{P}\, \mathrm{e}^{-\frac{\Theta}{2}\mathcal{H}}\, \hat{\mathcal{O}}\, \mathrm{e}^{-\frac{\Theta}{2}\mathcal{H}}\, \mathcal{P} \mid \Psi_n \rangle}{\sum_n \langle \Psi_n \mid \mathcal{P}\, \mathrm{e}^{-\Theta\mathcal{H}}\, \mathcal{P} \mid \Psi_n \rangle}\,, \tag{4}$$

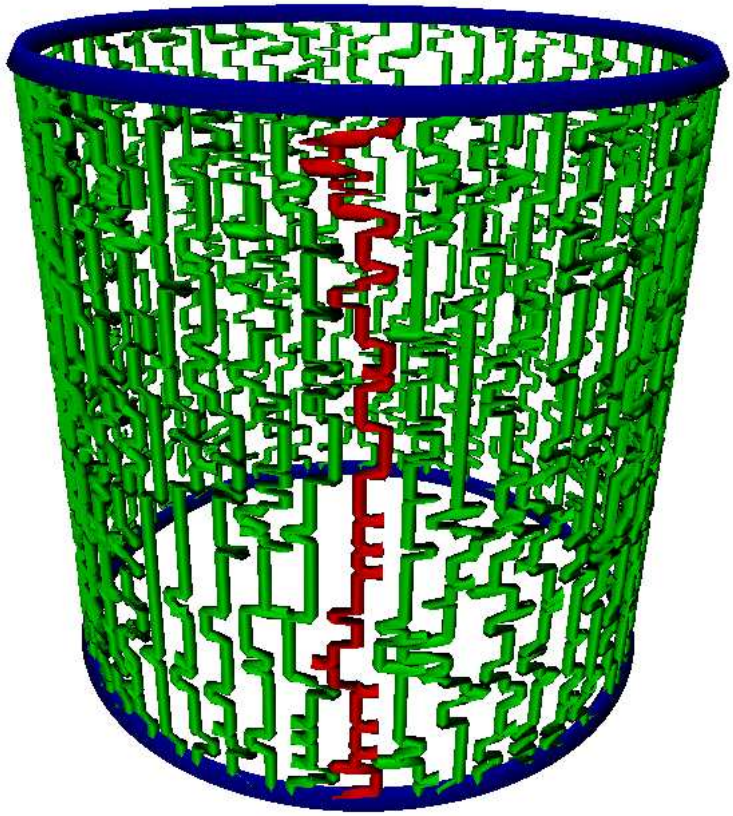

Figure 1. World-lines on a chain with periodic boundary conditions. World-lines that cross the boundary are marked in red.

where $\mid \Psi_n\rangle = \mid s_n\rangle \otimes \mid \Psi_T\rangle$, with $\{\mid s_n\rangle\}$ a complete set of spin states and $\mid \Psi_T\rangle$ a trial wavefunction for the spinless fermions. $\mathcal{P}$ is a projector ensuring the constraint against double occupancy. Taking the limit $\Theta \rightarrow \infty$ leads each state $\mathcal{P} \mid \Psi_T\rangle \otimes \mid s_n\rangle$ to converge to the ground-state (GS) as long as the GS has a finite overlap with it. The multiplicity is corrected by the normalization factor. Introducing after slicing in imaginary time (typically time slices $\Delta\tau = 0.1/t$ are used) a complete set of spin states, and checkerboarding, the spin states are represented by world-lines, and for each configuration of them, fermions are evolved exactly since the Hamiltonian (3) is bilinear in fermions. It can be easily shown that the total weight for a given configuration of the world-lines is given by $W_H D_f$, where W_H is the weight of an antiferromagnetic Heisenberg model (AFHM), whereas D_f is a fermionic determinant[10,11]. The updating of spin world-lines is performed using the loop-algorithm[18], with the same complexity as for an AFHM, in contrast to a recently proposed pure loop-algorithm[8]. In fact, the autocorrelation time ($\tau \sim 2$ for a system of length $L = 30$ and $J/t = 2$) for the internal energy is very similar to the one for the AFHM. Due to the combination of the loop-algorithm with the determinantal one, we denominate the whole hybrid-loop algorithm.

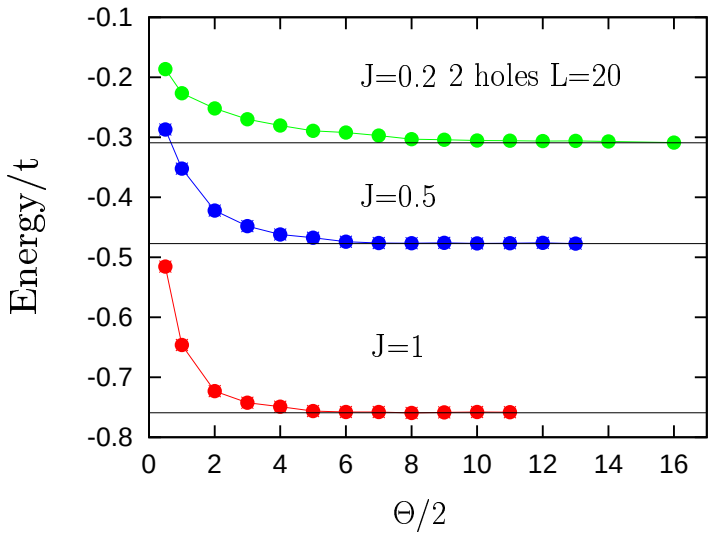

Figure 2. Ground-state energies vs. exact diagonalization results for $L = 20$ with two holes as a function of the projection parameter Θ.

Figure 2 shows a comparison of GS energies from QMC and exact diagonalization for various values of J at a density $n = 0.9$. The correct value is reached for values of the projection parameter $\Theta \sim 10/t - 20/t$, demonstrating that the algorithm leads to the correct GS with high accuracy (statistical errors are smaller than the size of the symbols). Dynamical data are obtained from the imaginary time Green's function and analytically continued using the maximum entropy method[19].

3 Results: Charge-Spin Separation in the One-Dimensional t-J Model

We focus first on the spectral function for one-particle excitations in the one-dimensional (1-d) NN t-J model[20], since in this case the present algorithm shows an average sign very close to one, such that a high accuracy, needed to produce dynamical data, could be easily reached. On the other hand, the 1-d NN t-J model has a phase with dominating superconducting correlation, a spin-gap phase, and also phase-separation[21], resembling thus many of the phases found in HTS.

It is well established that electrons in 1-d metals generally lead to a Luttinger liquid[22,23], where charge-spin separation (CSS) takes place. The most direct evidence of CSS was predicted for the spectral function of such systems[24]. An exact theoretical evaluation of the one-particle spectral function $A(k, \omega)$ could until now only be fully accomplished for the Hubbard model at $U = \infty$ for arbitrary doping on the basis of the Bethe-Ansatz solution[25]. However, recent progress was made for spectral properties of the supersymmetric (SuSy) t-J model with inversed squared (IS) interaction, where beyond the exact ground

state[26], the thermodynamics[27], the compact support of $A(k,\omega)$[28], the single-hole dynamics[29], and the electron addition spectrum[30] could be calculated analytically. In addition to spinons and holons, the IS SuSy t-J model was shown to contain antiholons with charge $Q = 2e$, spin $S = 0$, and twice the mass of the holons, i.e. they are not merely charge conjugate to the holons.

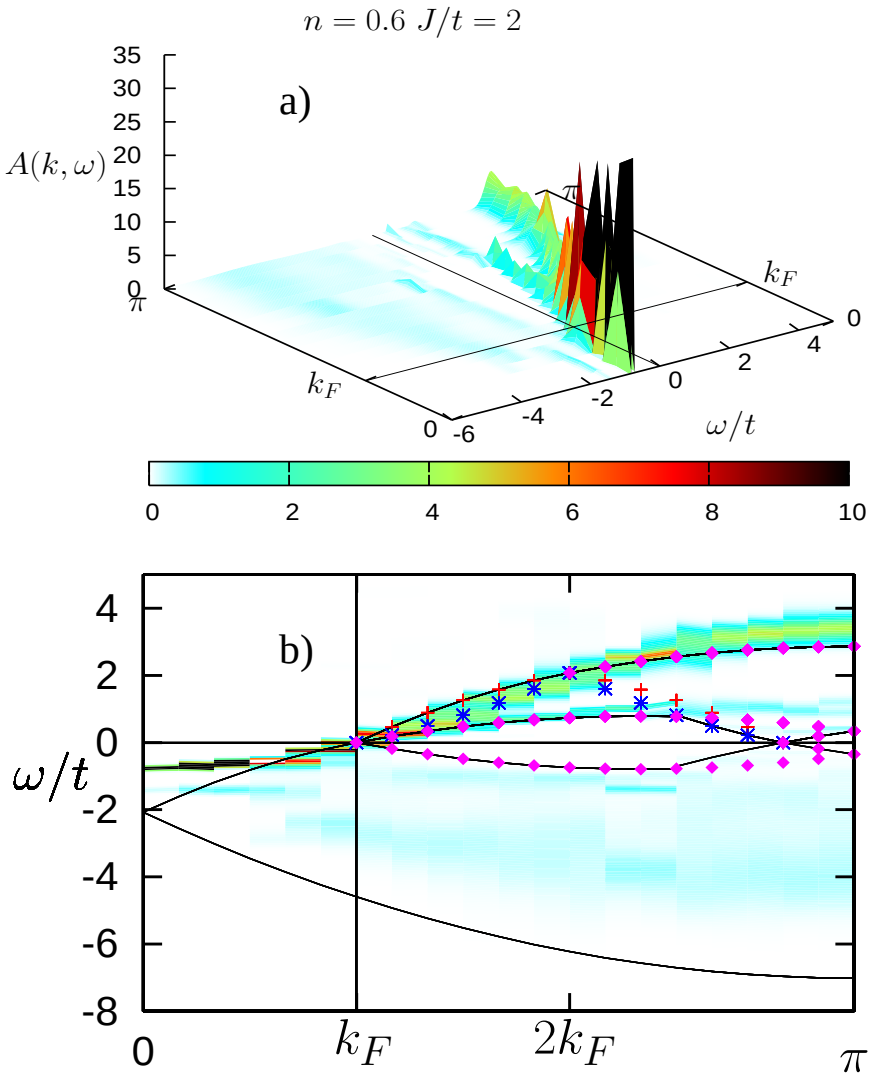

Figure 3. a) $A(k,\omega)$ for $J = 2t$ at a density $n = 0.6$. b) Projection of intensities on the (ω, k) plane. Solid lines: compact support of the IS SuSy t-J model. Red crosses: spinons, blue asterisks: holons, magenta diamonds: antiholons.

We consider $A(k,\omega)$ both for electron-removal (ER) and electron-addition (EA) processes. Figure 3 a) shows $A(k,\omega)$ obtained from the QMC simulations of the NN t-J model, Eq. (3), for $J = 2t$ (i.e. the SuSy point), at a density $n = 0.6$. The Fermi energy is taken as the zero of the energy scale. A splitting of the spectral weight into two branches can be readily seen on the EA side, in contradiction with what is expected for a simple metal. Figure 3 b) shows the projection of $A(k,\omega)$ on the (ω, k) plane, revealing the dispersion of the main features in the spectrum, together with the compact support for the IS SuSy t-J model at the same density. Furthermore, the dispersions of spinon (s), holon (h), and antiholon ($\bar{h}$) branches that determine the compact support for EA processes in the IS SuSy t-J model are also shown. The compact support is obtained by assuming that the energy and momenta of the particle (EA) or hole (ER) are given by the addition of energy and momenta of s, h, and $\bar{h}$. In the ER part of the spectrum, only the corresponding part of the compact support and the dispersion of an antiholon branch along the support is shown for clarity. A sharp feature is visible on the ER side that escapes from the compact support of the IS SuSy model. It is due to a holon branch, and as already discussed in the limit of a single hole[12], the actual dispersion of the holon is needed, in order to describe this feature correctly. Also a deviation from the IS SuSy compact support is observed on the EA side at high energies, where the differences in the models is expected to become noticeable. There are however, several features that are well described by the excitations of the IS model. The strongest feature on the EA side is followed closely by the spinon and holon branches between k_F and $2k_F$, and for $k > 2k_F$ by a spinon at k_F together with a dispersing antiholon. The analytic results for EA processes in the IS SuSy model[30] show that the largest portion of spectral weight is along this line. More striking is a second, weaker, but clearly visible branch that follows very closely the dispersion of an antiholon between k_F and $2\pi - 3k_F$. The analytic results of $A(k,\omega)$ for the IS SuSy model[30] predict a stepwise discontinuity at this edge and, in fact, the explicit evaluation of the weight shows for the present range of doping a higher value than in the interior of the support. Also the upper edge of the compact support on the ER part, that in the IS model corresponds to an antiholon, is well reproduced, with spectral weight down to very low energies around $3k_F$, as predicted by the IS SuSy model. Therefore, at the SuSy point, the clearest signal of CSS in $A(k,\omega)$ for the NN t-J model are present in the EA part of the spectrum and through the comparison with the IS t-J model, it is clear that a sizeable part of the spectral weight goes to the antiholon excitation.

Since the exact solution of the IS model is restricted to the SuSy point, it is of much interest to see whether the features discussed above correspond to a generic behavior of the NN t-J model. Figure 4 a) shows $A(k,\omega)$ for $n = 0.6$ and $J = 0.5t$, i.e. very far away from the SuSy point and at a value of J/t of experimental relevance for cuprate compounds. A perspective was chosen, so that it is already visible that as in the SuSy case, a structure splits off the main feature for k between $2k_F$ and π. Figure 4 b) shows the projection of $A(k,\omega)$ on the (ω, k) plane. As a model for free spinons, holons, and antiholons, we use the same dispersions as for the IS SuSy model, but with $\epsilon_{\mathrm{sR(L)}}(q) = (J/2)q(\pm v_{\mathrm{s}}^0 - q)$, i.e. assuming that away from the SuSy point, only the energy scale of spinons is changed. The corresponding compact support, spinon, holon, and antiholon dispersions are encoded as in Fig. 3. In the present case, the compact support encloses rather well all the spectral weight. Moreover, on the ER part, the strongest feature is very accurately followed by a spinon, whereas a second structure is also closely followed by a holon. On the EA side, the

feature with largest intensity is followed close to k_F by a holon, a spinon, and an antiholon. However, further away from k_F, the dispersion of the maximum is, up to $k \sim 2k_F$, closer to an antiholon going from k_F to $2\pi - 3k_F$ and beyond $2k_F$ by a curve corresponding to a spinon at k_F and a dispersing antiholon. Moreover, a second maximum develops

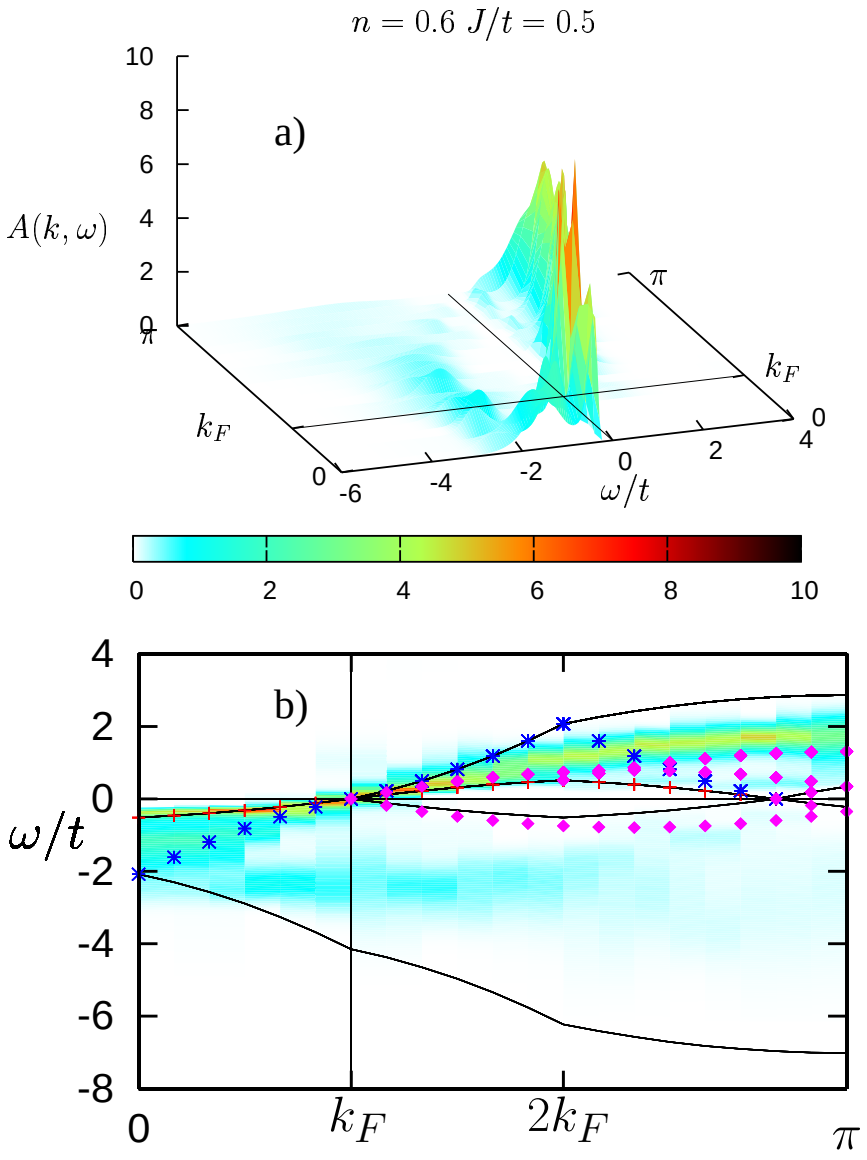

Figure 4. a) $A(k,\omega)$ for $J = 0.5t$ at $n = 0.6$. b) Projection of intensities on the (ω, k) plane. Symbols coded as in Fig. 3

beyond $2k_F$ that follows the antiholon dispersing from k_F to $2\pi - 3k_F$, in a similar way as for $J = 2t$ but with a smaller gap between both curves. In particular, the results from the simulations show appreciable weight between $3k_F$ and the zone boundary, where only antiholons are present.

A closer look to both features signaling CSS is given in Fig. 5. Figure 5 a) shows $A(k, \omega)$ on the ER side and the location of the excitation energies for one spinon and one holon. Whereas the spinon dispersion follows the QMC data very closely, a deviation is seen for the holon for the farthest points from k_F, as can be expected, since at higher energies, details of the dispersion matter in general. Yet, the agreement is good enough to enable an identification of the excitation content of the spectrum. The details of the

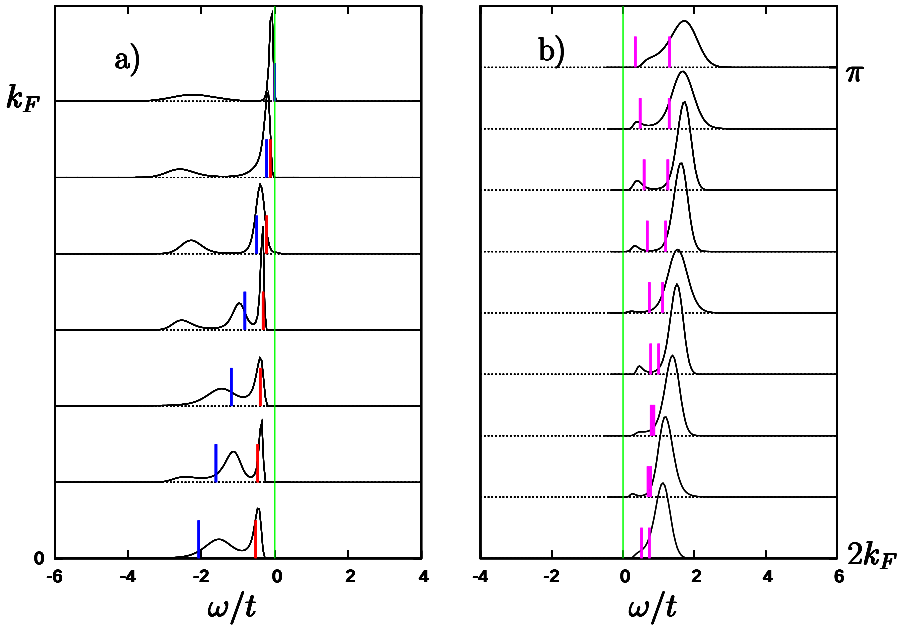

Figure 5. Detailed view of $A(k, \omega)$ at $J = 0.5t$ and $n = 0.6$. a) ER side for $0 \leq k \leq k_F$ at $J = 0.5t$ and $n = 0.6$. Vertical bars denote the positions for free spinon (closer to $\omega = 0$) and holon excitations. b) EA side for $2k_F \leq k \leq \pi$. Vertical bars denote here antiholon dispersions.

splitted maxima for $2k_F \leq k \leq \pi$ on the EA side are shown in Fig. 5 b), where both an antiholon dispersing from k_F to $2\pi - 3k_F$ (closer to $\omega = 0$) and an antiholon dispersing from $2k_F$ to $2\pi - 2k_F$ on top of a spinon at k_F are shown. Whereas the latter follows the larger maximum, the former can be associated with the second maximum. As at the SuSy point, there seems to be almost no weight associated with the left propagating spinon and holon that give rise to the contributions between $2k_F$ and $3k_F$. This is consistent with the analytic results obtained for the IS SuSy model[30]. Results for other values of doping ($0.6 \leq n \leq 0.9$) and J ($0.5 \leq J/t \leq 3$) not presented here, show the same qualitative behavior, in particular the presence of a branch on the EA side below the main dispersing structure, that is closely followed by an antiholon branch under the assumption of free spinons, holons, and antiholons.

4 Concluding Remarks

In summary, one-particle spectra for electron-removal and addition were obtained using a new algorithm that delivers accurate dynamical data for the nearest-neighbor t-J model. A comparison with the compact support and excitation content of the $1/r^2$ t-J model at the supersymmetric point $J = 2t$ shows that a new manifestation of charge-spin separation in the NN model can be observed in the EA part of the spectrum, where in addition to spinons and holons, a branch following the antiholon dispersion is clearly visible. The same feature is still visible at $J = 0.5t$, where assuming the same dispersions for the holon, and antiholon, as in the IS model but changing the scale of energy to J for the spinon, a fairly good description of the spectrum can be given. Instead, serious deviations result by omiting the antiholon or setting its mass equal to that of the holon (i.e. assuming that it is the charge conjugated counterpart of the holon). The results above strongly indicate, that antiholons, that are not charge conjugate of holons, are generic excitations in the nearest neighbor t-J model.

Acknowledgments

We are grateful to M. Brunner for important contributions at early stages of this project. We acknowledge interesting discussions with F.F. Assaad. We wish to thank HLR-Stuttgart (Project DynMet) and NIC-Jülich for allocation of computer time and SFB 382 for financial support.

References

1. G. J. Bednorz and K. A. Müller, *Possible High T_c Superconductivity in the Ba-La-Cu-O System*, Z. Phys. B **64**, 189-193 (1986).
2. *Correlated Electron Systems, Special Issue*, Science **288**, 461-480 (2000).
3. M. Imada, A. Fujimori, and Y. Tokura, *Metal-insulator transitions*, Rev. Mod. Phys. **70**, 1039-1263 (1998).
4. E. H. Lieb and F. Y. Wu, *Absence of Mott transition in an exact solution of the short range, one-band model in one dimension*, Phys. Rev. Lett. **20**, 1445-1448 (1968).
5. A. Georges, G. Kotliar, W. Krauth, and M. J. Rozenberg, *Dynamical mean-field theory of strongly correlated fermion systems and the limit of infinite dimensions*, Rev. Mod. Phys. **68**, 13-125 (1996).
6. E. Dagotto, *Correlated electrons in high-temperature superconductors*, Rev. Mod. Phys. **66**, 763-840 (1994).
7. F. F. Assaad and D. Würtz, *Charge and spin structures in the one-dimensional t-J model*, Phys. Rev. B **47**, 2681-2696 (1991).
8. B. Ammon, H. G. Evertz, N. Kawashima, M. Troyer, and B. Frischmuth, *Quantum Monte Carlo loop algorithm for the t-J model*, Phys. Rev. B **58**, 4304-4319 (1998).
9. M. Brunner and A. Muramatsu, *Quantum Monte Carlo simulations of infinitely strongly correlated fermions*, Phys. Rev. B **58**, R10100-R10103 (1998).
10. A. Muramatsu, *Quantum Monte Carlo for lattice fermions*, in *Quantum Monte Carlo Methods in Physics and Chemistry*, eds.: M. P. Nightingale and C. J. Umrigar, (Kluwer Academic Press, Dordrecht, 1999).

11. F. F. Assaad, *Quantum Monte Carlo Methods on Lattices: The Determinantal Approach*, in *Quantum Simulations of Complex Many-Body Systems: From Theory to Algorithms*, eds.: J. Grotendorst, D. Marx, and A. Muramatsu, NIC Series, Vol. 10 (2002).
12. M. Brunner, F. F. Assaad, and A. Muramatsu, *Single hole dynamics in the one-dimensional t-J model*, Eur. Phys. J. B **16**, 209-212 (2000).
13. M. Brunner, F. F. Assaad, and A. Muramatsu, *Single-hole dynamics in the t-J model on a square lattice*, Phys. Rev. B **62**, 15480-15492 (2000).
14. M. Brunner, S. Capponi, F. F. Assaad, and A. Muramatsu, *Single hole dynamics in the t-J model on two- and three-leg ladders*, Phys. Rev. B **63**, 180511(R) (2001).
15. S. Sorella and L. Capriotti, *Green function Monte Carlo with stochastic reconfiguration: An effective remedy for the sign problem*, Phys. Rev. B **61**, 2599-2612 (2000).
16. G. Khaliullin, JETP Lett. **52**, , (389)1990.
17. A. Angelucci, *Effective lattice actions for correlated electrons* Phys. Rev. B **51**, 11580-11583 (1995).
18. H. G. Evertz, *The Loop Algorithm*, Adv. Phys. **52**, 1 (2003).
19. M. Jarrell and J. Gubernatis, Phys. Rep. **269**, 133 (1996).
20. C. Lavalle, M. Arikawa, S. Capponi, F. F. Assaad, and A. Muramatsu, *Antiholons in One-Dimensional t - J Models*, Phys. Rev. Lett. **90**, 216401 (2003).
21. M. Ogata, M. U. Luchini, S. Sorella, and F. F. Assaad, *Phase diagram of the one-dimensional t-J model*, Phys. Rev. Lett. **66**, 2388-2391 (1991).
22. F. D. M. Haldane, J. Phys. C **14**, 2585 (1981).
23. J. Voit, Rep. Prog. Phys. **58**, 977 (1995).
24. V. Meden and K. Schönhammer, *Spectral functions for the Tomonaga-Luttinger model*, Phys. Rev. B **46**, 15753-15760 (1992).
25. K. Penc , K. Hallberg, F. Mila, and H. Shiba, *Shadow Band in the One-Dimensional Infinite-U Hubbard Model*, Phys. Rev. Lett. **77**, 1390-1393 (1996).
26. Y. Kuramoto and H. Yokoyama, *Exactly soluble supersymmetric t-J-type model with long-range exchange and transfer*, Phys. Rev. Lett. **67**, 1338-1341 (1991).
27. Y. Kuramoto and Y. Kato, J. Phys. Soc. Jpn. **64**, 4518 (1995).
28. Z. N. C. Ha and F. D. M. Haldane, *Elementary Excitations of One-Dimensional t-J Model with Inverse-Square Exchange*, Phys. Rev. Lett. **73**, 2887-2890 (1994).
29. Y. Kato, *Hole Dynamics of the One-Dimensional Supersymmetric t-J Model with a Long-Range Interaction: An Exact Result*, Phys. Rev. Lett. **81**, 5402-5405 (1998).
30. M. Arikawa, Y. Saiga, and Y. Kuramoto, *Electron Addition Spectrum in the Supersymmetric t-J Model with Inverse-Square Interaction*, Phys. Rev. Lett. **86**, 3096-3099 (2001).